applied sciences

MDPI

Article

Stress–Structural Failure of a 610 m Crushing Station Left-Side Tunnel Section in Jinchuan II Mine: A Numerical Simulation Study

Yongyuan Kou [1,2], Shenghua Yin [1,*], Shili Qiu [3] and Jie Xin [3]

[1] School of Civil and Resources Engineering, University of Science and Technology Beijing, Beijing 100083, China
[2] No. 2 Mining Area, Gansu Jinchuan Group Co., Ltd., Jinchang 737100, China
[3] State Key Laboratory of Geomechanics and Geotechnical Engineering, Institute of Rock and Soil Mechanics, Chinese Academy of Sciences, Wuhan 430071, China
* Correspondence: hyq2428204462@163.com

Abstract: To address the stress–structural failure phenomenon that can be induced by the excavation of a left-side tunnel section of a 610 m crushing station, an unmanned aerial vehicle was used in this study to collect the geological conditions and rock mass information of the working face, and important geometric information such as the attitude and spacing of rock mass were extracted. Based on the identified attitude and spacing information, a three-dimensional rock mass structure and numerical simulation model of the 610 m crushing station left-side tunnel section were constructed using discrete element numerical simulation software (3DEC) (version 5.0). The results show that the surrounding rock instability of the left-side tunnel section of the 610 m crushing station is controlled by both the stress field in the contact zone between reddish-brown granite stratum and the gray-black-gray gneiss stratum. The cause of stress–structural failure is that the joint sets (JSet #2 and JSet #3) are most likely to form unfavorable blocks with the excavation surface due to unloading triggered by the excavation. Therefore, stress–structural failure disasters in jointed strata sections are one of the key issues for surrounding rock stability during crushing station excavation. It is suggested to adopt 'optimized excavation parameters + combined support forms' to systematically control stress–structural failure after unloading due to the excavation from three levels: surface, shallow, and deep. The stress–structural failure mechanism of deep rock mass is generally applicable to a large extent, so the results of this research have reference value for engineering projects facing similar problems around the world.

Keywords: Jinchuan II mine; stress–structure failure; 3D reconstruction; numerical simulation

check for updates

Citation: Kou, Y.; Yin, S.; Qiu, S.; Xin, J. Stress–Structural Failure of a 610 m Crushing Station Left-Side Tunnel Section in Jinchuan II Mine: A Numerical Simulation Study. *Appl. Sci.* **2024**, *14*, 59. https://doi.org/10.3390/app14010059

Academic Editors: Stefano Invernizzi and Amin Beiranvand Pour

Received: 27 October 2023
Revised: 1 December 2023
Accepted: 19 December 2023
Published: 20 December 2023

1. Introduction

With rapid economic growth and increasing population base, China's demand for resource extraction is also growing. However, it also faces challenges such as resource depletion, environmental degradation, and safety hazards in production. Therefore, the trend of resource extraction in China is progressing in a green, efficient, and safe direction [1,2]. The Jinchuan II mine is one of the largest polymetallic deposits in China, with abundant resource potential and considerable development value in its deep ore bodies. However, as the mining depth increases, deep rock mass is subjected to the effects of 'three highs and one disturbance' (high ground stress, high ground temperature, high permeability pressure, strong mining disturbance), which leads to stress–structure failure phenomena. This not only affects mining efficiency and safety but also poses threats to underground engineering structures and underground/surface environments [3–5]. Thus, investigating the stress–structure failure phenomena and the underlying mechanisms in the left-side

tunnel section of the 610 m crushing station can provide theoretical guidance and technical support for deep mining in Jinchuan II mine.

Stress–structure failure, which refers to the sudden and unpredictable instability and collapse of a rock mass, is an important issue in deep-rock mechanics and mining theory, as well as one of the technical challenges in deep mining operations [6–8]. To date, domestic and foreign scholars have conducted extensive theoretical analyses, numerical simulations, experimental studies, and on-site monitoring regarding this issue, achieving notable results [9–22]. For example, Zhao et al. [10] established a stress analysis model for deep hard rock deposits and analyzed the influence of different factors on stress distribution. Hu [13] investigated the damage mechanism and instability of surrounding rock under deep high-stress conditions, and proposed a surrounding rock stability evaluation method based on damage variables. Yang et al. [16] discussed the critical technologies and countermeasures for backfill mining in high-stress ore bodies in large nickel mines and provided reasonable support measures and parameters. Xiao et al. [17] investigated stress–structure failure during the excavation process of the underground powerhouse of Baihetan hydropower station and found that tensile fracturing is the most active rock mass fracture mechanism in the evolution of stress–structure failure. Martin et al. [19] found that the Hoek–Brown brittleness parameter can be used to estimate the depth of brittle failure around a tunnel, supporting demand load caused by stress–structure-induced failure. Li et al. [21] found that when propagating cracks intersect existing joint sets, stress–structure rock bursts are considered structural failures and analyzed using a catastrophic model. However, there are still three research gaps concerning stress–structural failure induced by deep mining: (1) the lack of in-depth analysis and systematic summarization for specific mining areas or deposit conditions; (2) insufficient consideration of complex situations and nonlinear effects resulting from the comprehensive effects of multiple factors; (3) the lack of targeted prevention and control measures and suggestions. And, in the existing literature, there is no specific systematic, detailed, and comprehensive analysis and discussion regarding the stress–structural failure induced by deep mining in the left-side tunnel section of the 610 m crushing station at Jinchuan II mine.

Thus, to address the stress–structural failure phenomena that can be induced by the excavation in the left-side tunnel section of the 610 m crushing station, this research is based on the collection of geological conditions and rock mass information of the working face using unmanned aerial vehicles (UAVs); combined with the application of discrete element numerical simulation software (3DEC), a three-dimensional rock mass structure and numerical simulation model are constructed. And the research aims to investigate the deformation characteristics, failure mechanisms, and instability modes of a deep rock mass under high-stress conditions. Moreover, in light of the simulation results, measures and suggestions for preventing and controlling stress–structural failure in a deep rock mass are proposed. This can provide theoretical guidance and technical support for deep mining in Jinchuan II mine, as well as reference value for deep mining under similar conditions elsewhere.

2. 610 m Crushing Station

The 610 m crushing station is an important project constructed by Jinchuan II mine to improve production efficiency and reduce costs, as shown in Figure 1. This project is located at the 610 m horizontal plane and mainly extracts the middle and lower sections of the ore body. It is primarily distributed within the porphyry and the contact zone between the porphyry and surrounding rocks. And it exhibits irregular flattened or lens-like shapes and is found within multiple stages of fault structures; the main valuable elements are nickel, copper, cobalt, and platinum group elements, among others. The rocks in the 610 m crushing station are striped mixed rocks: light flesh red, granular metamorphic structure, and striped structure. The main mineral components are orthoclase, plagioclase, quartz, and hornblende, with partial chloritization. Some regional rocks are interspersed with clayey materials, and the engineering geological conditions are locally poor. The use of

high-strength and high-rigidity anchor bolt and cable support technology can effectively address the issue of rock mass instability under deep high-stress and fracture conditions. The construction of the 610 m crushing station has not only improved the ore-processing capacity and resource utilization rate but also saved energy consumption and transportation costs, reduced environmental pollution and safety risks, and laid a solid foundation for the sustainable development of Jinchuan II mine.

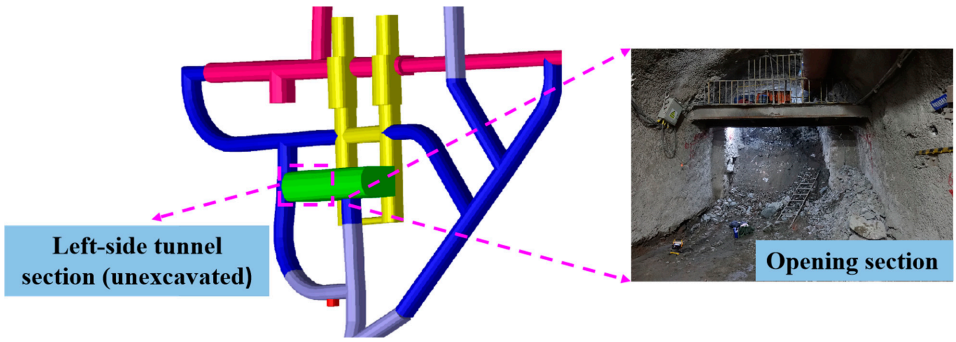

Figure 1. Information of 610 m crushing station.

3. Instability of the Crushing Station and Attitude of the Rock Mass

3.1. Stress–Structural Failure Phenomenon

During the excavation of the 610 m crushing station, stress–structural failure occurred, and the failure area was located in the opening section. This tunnel section mainly developed strata with alternating soft and hard layers of steeply inclined medium–thin-layered granite and gneiss. The on-site stress–structural phenomenon is illustrated in Figure 2. It can be observed that the loosening of blocks, opening of structural planes, and large block falling occurred on the right side of the working face and roof arch (facing the working face). An on-site investigation found that the freshly exposed working face has an obvious lithological interface. The right side of the lithological interface is gray-black gneiss (Figure 3a), which is distributed in the middle and right side of the roof arch, accounting for more than two-thirds of the working face area. The gneiss formation is characterized by a medium–thick-layered/blocky structure, and the rock mass minerals are mainly flaky black mica interspersed with fine quartz veins. The lower left portion of the interface is reddish-brown, medium-grained, altered granite (Figure 3b). The current exposed position of the working face is mainly concentrated on the left side of the roof arch. The minerals are mainly potassium feldspar and quartz, showing a medium–thick-layered structure with a compact texture. There are few interlayer planes, and joints cut the working face rock mass into flat hexahedral blocks. Based on the rock mass, surrounding rock failure, and support system damage revealed by on-site investigations, it can provide strong support for the construction of an unexcavated tunnel section in the left-side of the 610 m crushing station, ensuring its construction safety.

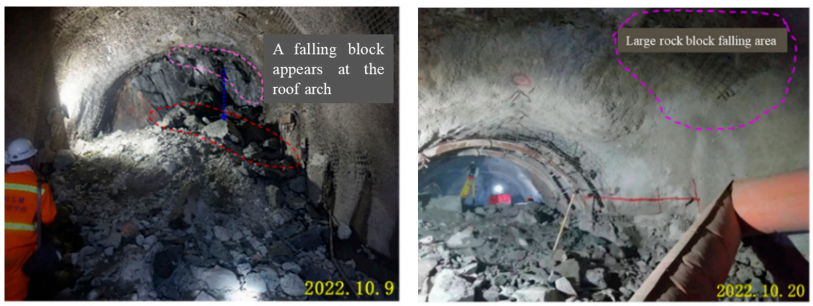

(**a**) (**b**)

Figure 2. Stress–structural failure of the 610 m crushing station: (**a**) A falling block appears at the roof arch; (**b**) failure area.

(**a**) (**b**)

Figure 3. Field sampling: (**a**) gray-black gneiss; (**b**) reddish-brown, medium-grained, altered granite.

3.2. Attitude of the Rock Mass

UAV technology and 3D reconstruction technology were used to obtain image information of the exposed rock mass surface of the 610 m crushing station working face, consistent with research results of Kong et al. [23]; i.e., a digital outcrop model generation method for rock exposures based on UAV-SfM photogrammetry was developed. And a high-precision and high-resolution 3D digital surface model of the 610 m crushing station was constructed (Figure 4). Important geometric information such as the attitude and spacing of structural planes (sets) of the rock mass was extracted (Figure 5). Through the statistical analysis of the structural attitude of the rock mass, a total of five dominant structural sets were identified and are listed in Table 1.

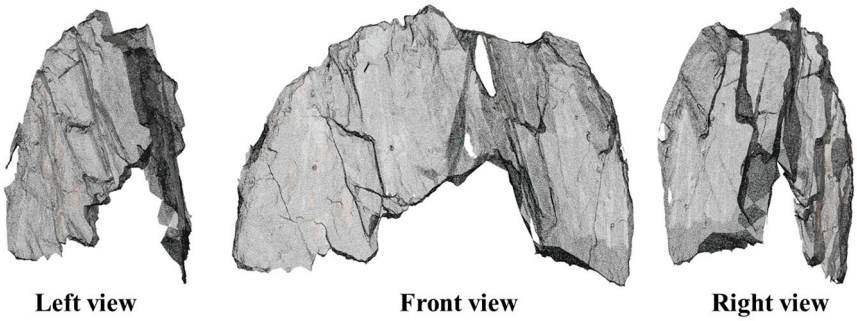

Figure 4. 3D reconstruction structure from motion (SFM) of rock mass structure.

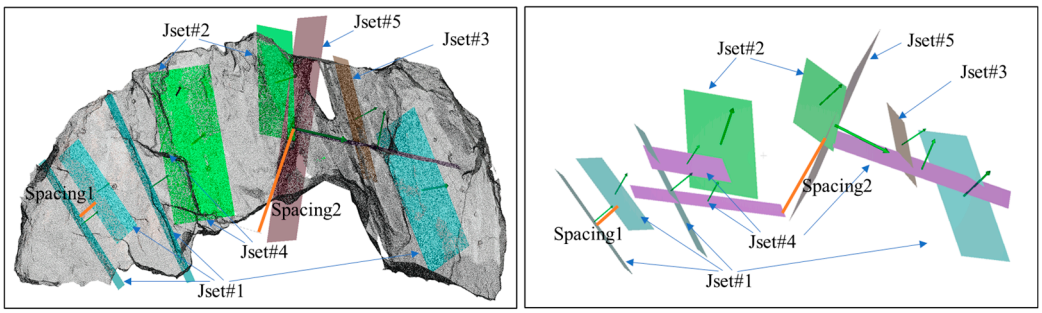

(**a**) (**b**)

Figure 5. 610 m crushing station working face structural plane identification: (**a**) structural plane (Jset) identification; (**b**) attitude and spacing measurement.

Table 1. Summary of dominant structural plane in mixed rock strata of 610 m crushing station.

Petrofabric Name	Lithology	Level, m	Structure Type	Attitude (Dip-Direction° (D-D)∠Dip° (D))				
				JSet #1	JSet #2	JSet #3	JSet #4	JSet #5
Migmatite zone	Granite, gneiss	610	Layered, layered–fractured	212∠57~63	220∠67~85	150∠66~85	70∠15~19	295∠75

The specific parameters for the dominant joint sets are as follows:

(1) JSet #1 is a joint set with an attitude of 212°∠57~63°, which is a typical interlayer joint set, as shown by the light-blue joint set in Figure 5b. The joint set is distributed in a granite formation and there is a relatively large spacing between the joint sets, ranging from 25 to 35 cm. It has a certain cohesion strength, and both the opening and closing properties are developed. The tensional joint surfaces are filled with muddy and sandy debris, while the closing joint surfaces exhibit an intermittent joint pattern.

(2) JSet #2 is a joint set with an attitude of 220°∠67~85°, which is a reverse dipping structural surface to the working face with a spacing of 25–55 cm. As shown in Figure 5, this structural surface (in light green) penetrates through both granite and gneiss strata, and intersects with joint sets JSet #2, #4, and #5, cutting out blocks on the working face. Additionally, the joint surfaces of this joint set are smooth and exhibit striations.

(3) JSet #3 is a joint set with an attitude of 150°∠67~85°. In the model constructed in Figure 5, three joints of this set (in light gray) are identified with a spacing of over 20 cm. It has a dip direction parallel to the working face and also intersects with the oblique interlayer joint set (JSet #3), which is more developed in the gneiss formation.

(4) JSet #4 is a joint set (in light purple) with an attitude of 70°∠15~19°. It is mainly developed in the gneiss strata, with some incisions into the granite strata near the lithological contact zone, but quickly terminates. The spacing between joint sets varies significantly and exhibits a certain degree of randomness. And the spacing ranges from 25 to 45 cm in Figure 5.

(5) JSet #5 (in purple red) has an attitude of 295°∠75°. It is mainly developed in the gneiss strata, with some incisions into the granite formation near the lithological contact zone, but quickly terminates. As shown in Figure 5, the spacing between joint sets varies significantly and exhibits a certain degree of randomness. The structure of this joint set is closed without any obvious filling materials.

4. Analysis of the Instability Mechanism in the 610 m Crushing Station

4.1. Principles of the Numerical Simulation

3DEC is a piece of 3D numerical simulation software that can be used to simulate the response of discontinuous media under static or dynamic loads such as rock underground engineering excavation, rock slope instability, rock foundation engineering, and masonry structure analysis [24,25]. Its numerical method is based on the discrete element method, which divides discontinuous media into multiple rigid or deformable blocks and describes the interactions between blocks through contact models. The contact models can consider normal and tangential forces, effects like friction and cohesion, as well as the geometric characteristics and material properties of the contact surfaces. The blocks can be described using either built-in material models or user-defined material models to depict the stress–strain relationship within the blocks. Additionally, 3DEC software adopts an explicit time integration method to solve the motion equations and employs iterative algorithms to update contact states and forces [26–28].

4.2. Numerical Model of the Left-Side Tunnel Section of the 610 m Crushing Station

To analyze the mechanism of stress–structural failure in the left-side tunnel section of the 610 m crushing station and identify the key controlling factors, a 3D rock mass structure and numerical simulation model of the left-side tunnel section were constructed using the

explicit discrete element method (3DEC) (Figure 6). The model was then used to simulate the excavation of the left-side tunnel section. The model dimensions (length, width, and height) were 50.0, 16, and 50.0 m, respectively. In order to reduce the boundary effect and increase calculation efficiency, the focused research area was divided around the model tunnel, with dimensions of 20.0 m × 16 m × 20.0 m. The size of the excavation tunnel section is shown in Figure 6, and joint sets are defined within the focused research area.

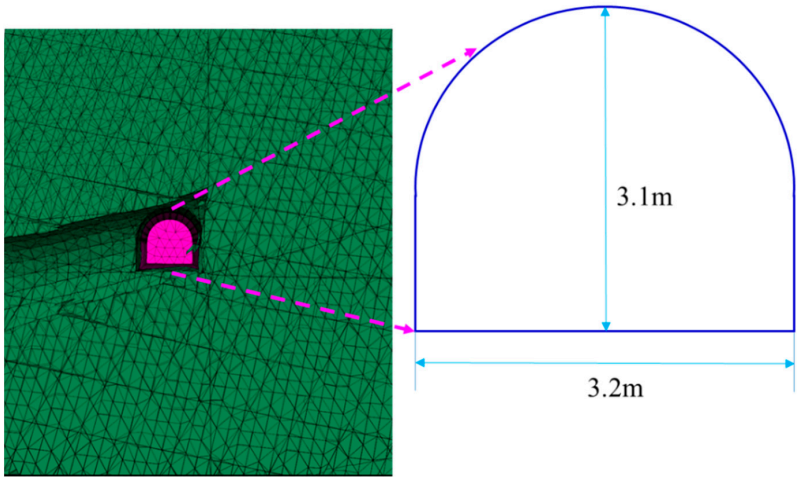

Figure 6. Three-dimensional numerical calculation model (3DEC).

4.3. Geo-Stress and Displacement Boundary Conditions

For the numerical simulation of the left-side tunnel section of the 610 m crushing station in Jinchuan II mine, the boundary conditions for geo-stress and displacement were set based on the on-site geological conditions. Specifically, according to the 'Engineering geological analysis and surrounding rock stability study of the 610 m crushing station project in Jinchuan II Mine' and combined with mechanical parameter inversion, the values of the geo-stress σ_x, σ_y, and σ_z in the numerical model were determined to be 42.16 MPa, 25.00 MPa, and 15.52 MPa, respectively. To simulate the real geo-stress environment, corresponding displacement constraints were applied at the boundaries of the model. Specifically, the velocity vectors of the blocks on the model boundaries were constrained to zero throughout the simulation process, thereby ensuring that the simulation conditions were consistent with the site conditions.

4.4. Joint Set and Mechanical Parameters

4.4.1. Geometric Parameters of the Joint Set

Based on on-site investigations and the identification of joint planes in Section 3.2, the numerical model was set up accordingly, taking into account the lithological interface and joint planes at the 610 m crushing station. The geometric parameters of the identified joint planes and lithological interfaces are shown in Table 2, and the joint settings in the model are shown in Figure 7.

Table 2. Joint set parameter setting information table in 3DEC.

Type	Set Number	Attitude (D-D °∠Dip °)	Face-Centered Coordinates	Joint Spacing, m	Joint Distribution
Lithologic interface	JSet#1	212∠63	(−1.0, 7.0, 2.0)	—	Granite–gneiss interface
Joint plane	JSet#2	329∠77	(−0.72, 7.55, 3.26)	0.41	Gneiss
	JSet#3	181∠69	(−0.09, 7.32, 4.07)	0.48	Gneiss
	JSet#4	271∠66	(−0.71, 7.46, 2.55)	1.34	Gneiss
	JSet#5	190∠19	(1.35, 7.36, 3.13)	1.83	Gneiss

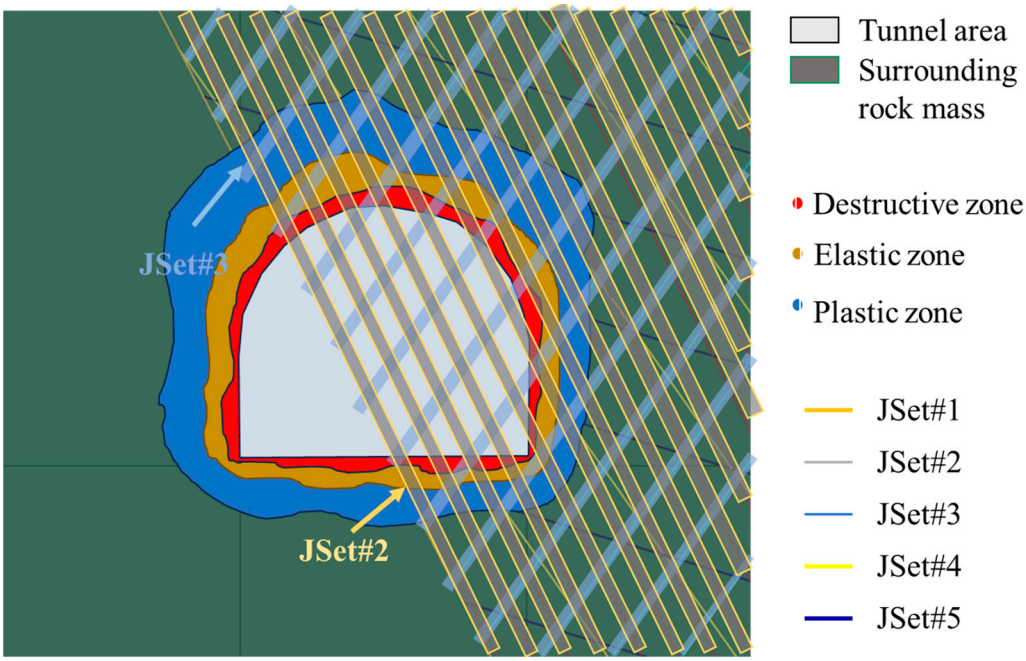

Figure 7. The joint setting in 3DEC.

4.4.2. Mechanical Parameters

Based on 'Engineering geological analysis and surrounding rock stability study of the 610 m crushing station project in Jinchuan II Mine', the mechanical parameters of the model were initially considered and then optimized to achieve consistency between the simulation results and the on-site investigation results. The Mohr–Coulomb constitutive model was adopted for both the blocks and joints, and the rock mechanical parameters and joint mechanical parameters are shown in Tables 3 and 4.

Table 3. Mechanical parameters of rock mass in 3DEC.

Lithology	Elasticity Modulus, GPa	Poisson's Ratio	Cohesion, MPa	Friction Angle, °	Tensile Strength, MPa	Dilatancy Angle, °
Granite	40.43	0.24	6.07	33.57	5.10	0.00
Gneiss	30.69	0.26	0.41	31.79	0.81	10.00

Table 4. Joint mechanical parameters in 3DEC.

Joint Position	Normal Stiffness, GPa	Shear Stiffness, GPa	Cohesion, MPa	Friction Angle, °	Tensile Strength, MPa	Dilatancy Angle, °
Interface	10.00	10.00	0.30	30.00	0.60	10.00
Gneiss	10.00	10.00	0.20	30.00	0.60	10.00

4.5. Analysis of the Instability Mechanism

4.5.1. The Migration Law of Working Face Blocks

As per Figure 8, the numerical simulation in the left-side tunnel section of the 610 m crushing station reveals noticeable displacements in the left and right sidewalls, as well as the floor, following excavation. These displacements occur in the direction of the positive Y-axis for the sidewalls, the negative Y-axis for the floor, and the positive Z-axis. Specifically, from the cross-sectional displacement contour diagram of the left-side tunnel section in Figure 8a, it can be seen that the middle area of the tunnel floor has a larger displacement value compared to other areas, and the distribution of large displacements extends inward to a depth of 1.0–2.0 m. In terms of the distribution range, the area with the largest

displacement is from the tunnel floor to the left and right sidewalls, and then to the roof arch area. The reason for the distribution of larger displacements is due to the interaction between joint sets (JSet #2 and JSet #3), as shown in Figure 7, in relation to the excavation face. This interaction results in a significant displacement of the rock mass, exerting major control on the movement of the blocks in this section. According to the displacement and velocity vectors in the left-side section of the 610 m crushing station shown in Figure 8b, there are signs of sliding and collapsing of the blocks formed by joint sets on the working face towards the free surface. This phenomenon is mainly concentrated in the middle area of the working face. Additionally, apart from the potential occurrence of block sliding and collapsing on the working face, the blocks in the area from the tunnel floor to the left and right sidewalls are also experiencing sliding and collapsing phenomena.

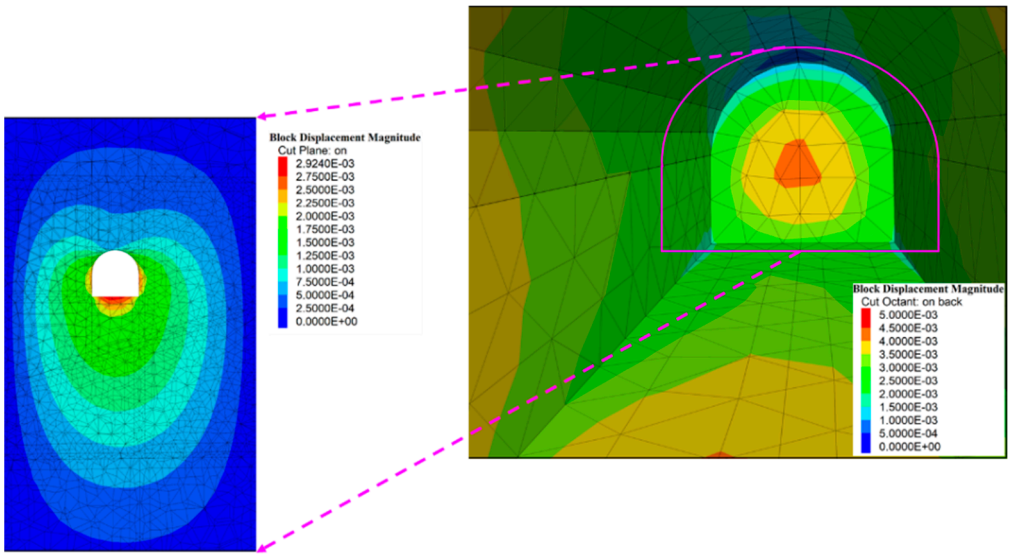

(**a**)

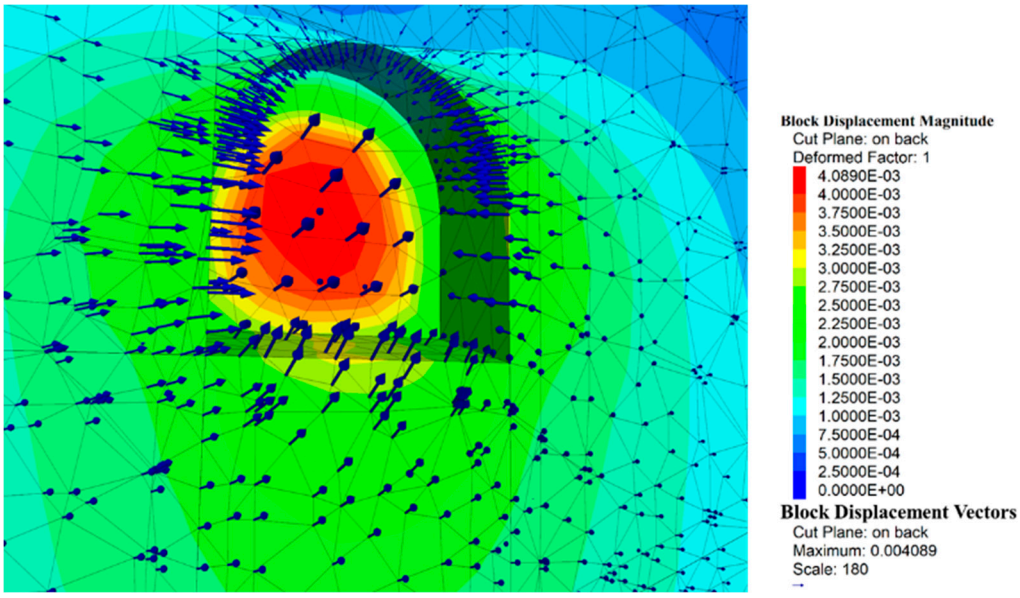

(**b**)

Figure 8. The left-side tunnel section of 610 crushing station: (**a**) displacement nephogram and the displacement cross-section nephogram (the section is 0.5 m from working face); (**b**) displacement and velocity vector diagram.

4.5.2. The Mechanism of Stress–Structure Interaction around the Tunnel

The maximum/minimum principal stress around the tunnel controls the location and depth of the surrounding rock failure and affects the movement mode of the rock mass [29–33], which is supported by the research of Xiao et al. [17], in particular the stress–structural failure (the maximum stress concentrations) occurring during the excavation process in the Baihetan hydropower station in China. The distribution of maximum/minimum principal stress around the left-side tunnel section of the 610 m crushing station tunnel is shown in Figure 9.

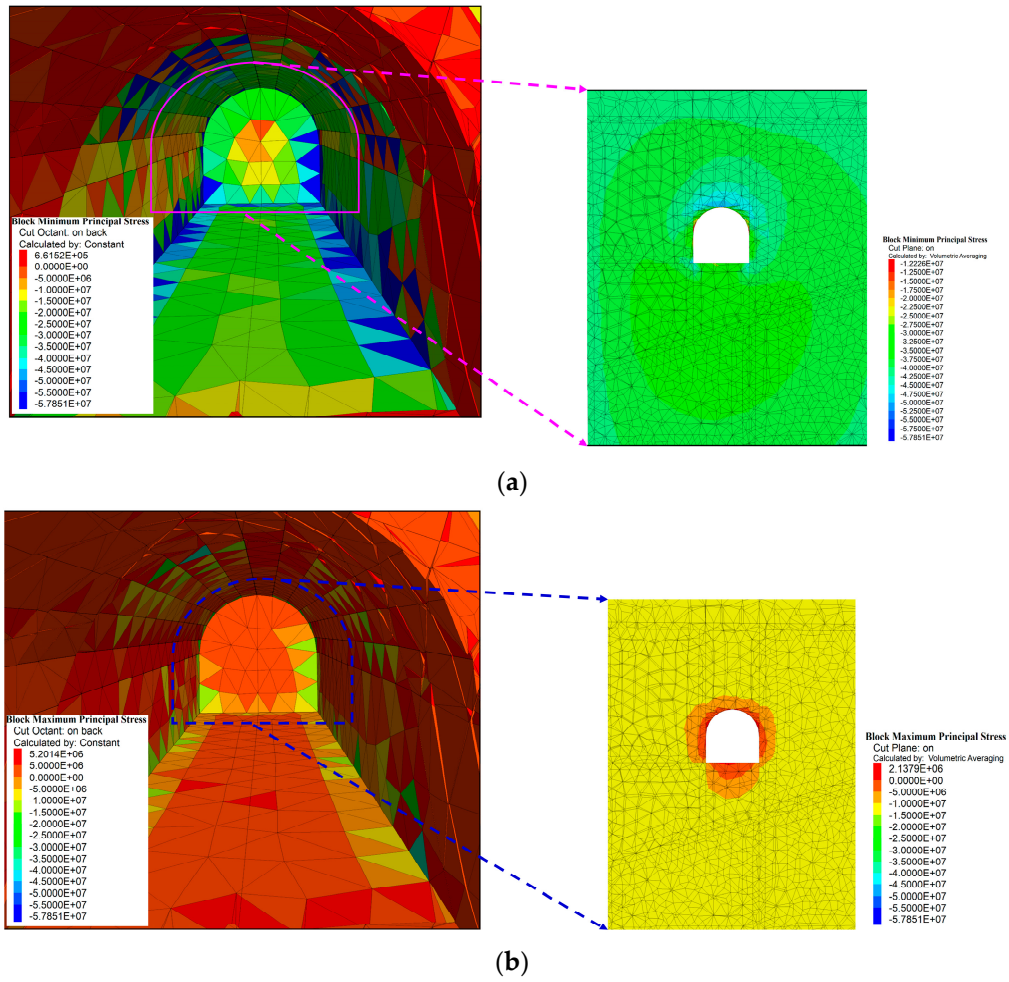

Figure 9. The left-side tunnel section of 610 m crushing station: (**a**) the maximum principal stress of left-side tunnel section and the maximum principal stress nephogram of cross-section (the section is 0.5 m from working face); (**b**) the minimum principal stress of left-side tunnel section and the minimum principal stress nephogram of the cross-section (the section is 0.5 m from working face).

The distribution of the maximum principal stress results (Figure 9a) indicates that due to tunnel excavation, there is stress unloading. Within the depth range of 5.0 m from the left and right sidewalls of the tunnel, the maximum principal stress values are mostly between 20 and 35 MPa. On the other hand, the maximum principal stress values on both sides of the tunnel roof arch are mostly between 12 and 17 MPa. At a depth of approximately 2 m from the bottom of the roof arch and the left and right sidewalls, there is a certain degree of stress concentration, with the maximum principal stress values ranging from 50 to 55 MPa. The distribution of the minimum principal stress reveals a pattern of stress relaxation in the surrounding rock (Figure 9b). The depths at which the lowest values of the minimum principal stress are distributed can reach up to 2.8 m in the tunnel perimeter area.

4.5.3. Damage Distribution Law of the Excavation

The formation of an excavation's damaged zone in the surrounding rock is closely related to the stress redistribution, rock conditions, and support methods. Fan et al. [34] used the surrounding rock damage zone to characterize the stress–structural failure in Jinping II diversion tunnels. This paper adopted a similar approach, and the distribution of the excavation damaged zone in the surrounding rock and the displacement vector diagram are shown in Figure 10. From Figure 10, it can be observed that the deepest portion of the damaged zone is mainly concentrated on the right sidewall, reaching a depth of 2.8 m. The depth of the damaged zone near the roof arch is mostly around 2.2 m, while it is around 1.5 m near the tunnel floor. The rock mass damage is mainly in the form of shear failure, with some zones experiencing tensile failure. The tensile failure zones are mostly on the right side of the roof arch, the lower portion of the left and right sidewalls. From Figure 10c, it can be seen that the locations with larger block displacements are mainly concentrated in the left and right sidewalls and the floor area of the tunnel, and there is also some contraction towards the free face of the tunnel in the perimeter area.

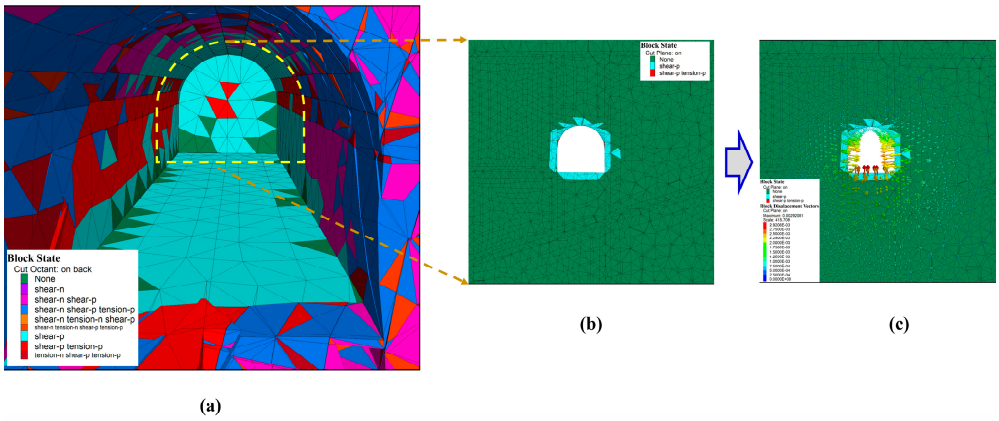

Figure 10. The left-side tunnel section of 610 m crushing station: (**a**) the distribution of excavation damage zone of surrounding rock; (**b**) excavation damage zone distribution and displacement vector diagram (section is 0.5 m from working face); (**c**) displacement vector local amplification diagram.

5. Conclusions

The stress–structural failure mechanism that occurs in the excavation of the left-side tunnel section of 610 m crushing station in Jinchuan II mine is investigated herein. The main causes and key controlling factors contributing to the formation of the mechanism and failure characteristics are discussed. The main conclusions, suggestions, and future research directions are as follows:

The instability of the surrounding rock in the left-side tunnel section of the 610 m crushing station is controlled by the contact area between the reddish-brown granite stratum and the gray-black-gray gneiss stratum, as well as the in-situ stress field. The stress–structural inducement is that the excavation and unloading of the crushing station causes joint sets (JSet #2 and JSet #3), and the excavation face causes the formation of unfavorable blocks. Thus, stress–structural failure caused by jointing in the formation of the tunnel section is one of the key issues concerning the instability of the surrounding rock during the excavation of the crushing station. To ensure overall stability during the excavation of the left-side tunnel section of the 610 m crushing station, it is recommended to adopt an 'optimized excavation parameter + joint support form' approach to systematically control stress–structural failure at three levels: the surface layer, shallow layer, and deep layer. The following specific measures are recommended: controlling the dosage of explosives used for excavation by blasting; reinforcing advanced support with anchoring; strengthening the surface layer with steel arches and shotcrete; and strictly limiting sidewall damage.

The perspective in future research about stress–structural failure in deep engineering should be centered on advancing the understanding of underground rock mechanics and structural behavior, with a clear goal of enhancing safety and operational reliability. Several key areas of focus can be considered: advanced numerical simulation techniques (discrete element and computational fluid dynamics); material characterization and modeling (the development of constitutive models that capture the complex behavior of rock under high-stress conditions); in-situ monitoring and instrumentation (advancements in sensor technology and real-time monitoring systems); and in-situ monitoring and instrumentation.

Author Contributions: Y.K.: conceptualization, methodology, and resources; S.Y.: conceptualization; S.Q.: formal analysis; J.X.: supervision. All authors have read and agreed to the published version of the manuscript.

Funding: This research was supported by the National Key R&D Program of China (Grant Nos. 2022YFC2904103); the Key Program of the National Natural Science Foundation of China (52034001); the Program of the National Natural Science Foundation of China (52004152); and the Youth Foundation of the Shandong Natural Science Foundation (ZR2020QE100).

Institutional Review Board Statement: Not applicable.

Informed Consent Statement: Not applicable.

Data Availability Statement: All data generated or analyzed during this study are included in this published paper.

Conflicts of Interest: Yongyuan Kou was employed by Gansu Jinchuan Group Co., Ltd. The remaining authors declare that the research was conducted in the absence of any commercial or financial relationships that could be construed as a potential conflict of interest.

References

1. Fang, Y.; Zhang, W.; Cao, J.; Zhu, L. Analysis on the current situation and development trend of energy resources in China. *Conserv. Utili. Mineral. Resour.* **2018**, *4*, 34–42.
2. Tang, L. Global energy supply versus demand: Current status and growth curve. *Int. Pet. Econ.* **2005**, *13*, 30–33.
3. Fan, D.; Li, F.; Wang, Z.; Miao, Q.; Bai, Y.; Liu, Q. Development status and prospects of China's energy minerals under the target of carbon peak and carbon neutral. *China Min. Mag.* **2021**, *30*, 1–8.
4. Li, X.; Zhou, J.; Wang, S.; Liu, B. Review and practice of deep mining for solid mineral resources. *Chin. J. Nonferrous Met.* **2017**, *27*, 1236–1262.
5. Yang, C.; Wang, T. Advance in deep underground energy storage. *Chin. J. Rock. Mech. Eng.* **2022**, *41*, 1729–1759.
6. LI, J.; Zhang, R.; Huang, L.; Zou, Y.; Fang, Y. Study on instability mechanism and disposal measures of brittle fractured surrounding rock area in high geo-stress tunnel. *Chin. J. Undergr. Space Eng.* **2018**, *14*, 1345–1351.
7. Lu, Z.; Ju, W.; Gao, F.; Zhang, Q.; Yi, k.; Sun, Z.; Yuan, G.; Dong, S. Experimental and numerical simulation research on intermittent failure of structural coal. *Chin. J. Rock Mech. Eng.* **2020**, *39*, 971–983.
8. He, M. Present situation and prospect of rock mechanics in deep mining engineering. In *Proceedings of the 8th National Academic Conference on Rock Mechanics and Engineering*; Springer: Singapore, 2004; pp. 88–94.
9. Zhao, J.; Feng, X.; Wang, P.; Jiang, Q.; Chen, B.; Zhou, Y.; Bei, S. Analysis of microseismic characteristics and fracture mechanism of underground caverns induced by blasting excavation. *Rock Soil Mech.* **2018**, *39*, 2563–2573.
10. Zhao, X.; Zhang, S.; Yang, X.; Zhou, X. Basic theory and calculation method of mining induced stress of deep hard rock deposits. *Mod. Min.* **2018**, *34*, 24–27.
11. Fan, Q. A Study of Stability of Deeply-Embedded Large-Diameter Cylindrical Structure in Soft Ground. Ph.D. Thesis, Dalian University of Technology, Dalian, China, 2005.
12. Hu, W.; Tan, X.; Jiang, Y.; Mao, J. A study of the mechanism and regularity of failures in the surrounding rock of a deep buried bias tunnel embedded in geologically bedding strata: Taking one tunnel of the Zhengwan line as an example. *Hydrogeol. Eng. Geol.* **2020**, *47*, 60–68.
13. Hu, N. Damage Mechanism and Stability Analysis of Stope Surrounding Rock under Deep High In-Situ Stress Condition. Ph.D. Thesis, University of Science and Technology Beijing, Beijing, China, 2021.
14. Ma, F.; Lu, R.; Guo, J.; Zou, L.; Kou, Y. Deformation analysis of large backfill by three-dimensional numerical simulation in No. 2 zone of Jinchuan mine. *J. Eng. Geol.* **2019**, *27*, 14–20.
15. Liu, L. Problems and countermeasures for safe and effective filling mining in Jinchuan Nickel mine in the deep and high stress. *Chem. Manage.* **2016**, *14*, 167.
16. Yang, Z.; Gao, Q.; Chen, D.; Guo, H. Problems and countermeasures for safe and effective filling mining in Jinchuan Nickel mine in the deep and high stress. *Strategic. Study. CAE.* **2014**, *16*, 38–44.

17. Xiao, Y.; Feng, X.; Feng, G.; Liu, H.; Jiang, Q.; Qiu, S. Mechanism of evolution of stress–structure controlled collapse of surrounding rock in caverns: A case study from the Baihetan hydropower station in China. *Tunn. Undergr. Space Technol.* **2016**, *51*, 56–67. [CrossRef]
18. Duan, Y.; Feng, X.; Li, X.; Ranjith, p.; Yang, B.; Gu, L.; Li, Y. Investigation of the effect of initial structure and loading condition on the deformation, strength, and failure characteristics of continental shale. *Geomech. Geophys. Geo-Energy Geo-Resour* **2022**, *8*, 207. [CrossRef]
19. Martin, C.; Kaiser, P.; McCreath, D. Hoek-Brown parameters for predicting the depth of brittle failure around tunnels. *Can. Geotech. J.* **1999**, *36*, 136–151. [CrossRef]
20. Lu, W.; Zhu, Z.; He, Y.; Que, X. Strength characteristics and failure mechanism of a columnar jointed rock mass under uniaxial, triaxial, and true triaxial confinement. *Rock Mech. Rock Eng.* **2021**, *54*, 2425–2439. [CrossRef]
21. Li, T.; Ma, C.; Zhu, M.; Meng, L.; Chen, G. Geomechanical types and mechanical analyses of rockbursts. *Eng. Geol.* **2017**, *222*, 72–83. [CrossRef]
22. Hadjigeorgiou, J.; Esmaieli, K.; Grenon, M. Stability analysis of vertical excavations in hard rock by integrating a fracture system into a PFC model. *Tunn. Undergr. Space Technol.* **2009**, *24*, 296–308. [CrossRef]
23. Kong, D.; Saroglou, C.; Wu, F.; Sha, P.; Li, B. Development and application of UAV-SfM photogrammetry for quantitative characterization of rock mass discontinuities. *Int. J. Rock Mech. Min. Sci.* **2021**, *141*, 104729. [CrossRef]
24. Zhou, Z.; Cao, P.; Lin, H. Selection of mechanical parameters of jointed rock mass in 3DEC application. *West-China Explor. Eng.* **2006**, *18*, 163–165.
25. Zhang, P.; Nordlund, E. A 3DEC numerical analysis of the interaction between an uneven rock surface and shotcrete lining. *Rock Mech. Rock Eng.* **2021**, *54*, 2267–2289. [CrossRef]
26. Deng, X.; Zhu, J.; Chen, S.; Zhao, J. Some fundamental issues and verification of 3DEC in modeling wave propagation in jointed rock masses. *Rock Mech. Rock Eng.* **2012**, *45*, 943–951. [CrossRef]
27. Zheng, Q. Analysis of Mountain Tunnel Seismic Damage and Study on Dynamic Response of Tunnel Entrance. Ph.D. Thesis, Southwest Jiaotong University, Chengdu, China, 2010.
28. Potyondy, D.; Cundall, P. A bonded-particle model for rock. *Int. J. Rock Mech. Min. Sci.* **2004**, *41*, 1329–1364. [CrossRef]
29. Xin, J.; Jiang, Q.; Li, S.; Chen, P.; Zhao, H. Fracturing and energy evolution of rock around prefabricated rectangular and circular tunnels under shearing load: A comparative analysis. *Rock Mech. Rock Eng.* **2023**, *56*, 9057–9084. [CrossRef]
30. Xin, J.; Jiang, Q.; Gong, F.; Liu, L.; Liu, C.; Liu, Q.; Yang, Y.; Chen, P. Mechanical behaviors of backfill-rock composites: Physical shear test and back-analysis. *J. Rock Mech. Geotech. Eng.* 2024; *in press*. [CrossRef]
31. Fang, Z.; Liu, L.; Zhang, X.; Han, K.; Wang, J.; Zhu, M.; Sun, W.; He, W.; Gao, Y. Carbonation curing of modified magnesium-coal based solid waste backfill material for CO_2 sequestration. *Process Saf. Environ. Prot.* **2023**, *180*, 778–788. [CrossRef]
32. Xie, G.; Suo, Y.; Liu, L.; Yang, P.; Qu, H.; Zhang, C. Pore characteristics of sulfate-activated coal gasification slag cement paste backfill for mining. *Environ. Sci. Pollut. Res.* **2023**, *30*, 114920–114935. [CrossRef]
33. Xie, G.; Liu, L.; Suo, Y.; Zhu, M.; Yang, P.; Sun, W. High-value utilization of modified magnesium slag solid waste and its application as a low-carbon cement admixture. *J. Environ. Manag.* **2024**, *349*, 119551. [CrossRef]
34. Fan, Y.; Zheng, J.; Cui, X.; Leng, Z.; Wang, F.; Lv, C. Damage zones induced by in situ stress unloading during excavation of diversion tunnels for the Jinping II hydropower project. *Bull. Eng. Geol. Environ.* **2021**, *80*, 4689–4715. [CrossRef]